

Threshold effects for quantum transport in multiterminal nanostructures

Bogdan R. Bułka

Institute of Molecular Physics, Polish Academy of Sciences, ul. M. Smoluchowskiego 17, 60-179 Poznań, Poland

Arturo Tagliacozzo

INFN-CNR "Coherentia" and Dipartimento di Scienze Fisiche, Università di Napoli "Federico II,"

Monte S. Angelo-via Cintia, I-80126 Napoli, Italy

(Received 20 November 2008; revised manuscript received 5 January 2009; published 20 February 2009)

The quantum conductance in a submicron T-junction structure is reconsidered here, within a single-particle linear-response scattering approach. We find that when a new conduction channel opens to conduction in a side terminal, the main source-drain conductance acquires a singularity that can be traced back to the so called "Wigner cusp," first encountered in nuclear cross sections. The shape of the singularity can be changed by tuning the gate voltages and can justify structures of the conductance measured in recent experiments involving nanodevices with similar geometry.

DOI: [10.1103/PhysRevB.79.075436](https://doi.org/10.1103/PhysRevB.79.075436)

PACS number(s): 73.23.-b, 73.63.Rt, 85.35.Ds, 85.35.Be

I. INTRODUCTION

Present lithography allows the fabrication of adjacent nanostructures with a spatial separation on the order of 100 nm. Quantum point contacts (QPCs) are used for detecting a flow of current through a device or for sensing the charge in a quantum dot (QD) nearby.¹ When used as a detector of the charge in a QD, the QPC is capacitively coupled to the QD, but it is not uncommon to couple it capacitively to a quantum wire (QW), e.g., to study Coulomb drag² or to allow for multiterminal nanostructures.³ In these cases it is important to take care of the back action of the detector on the system that one wants to measure.⁴ When using a QPC as a detector, it is common to polarize its conductance by means of gates close to the pinch-off point to exploit the strong nonlinearity in the current across the QPC at the opening of the conduction channel. Conductance in neighboring terminals may show intriguing behavior when one of them is polarized with gates close to the pinch-off voltage. Recent experiments^{5,6} show an enhancement of the conductance in one wire when side gate voltages drive another terminal across a conductance threshold. This also happens in simple cases when charging effects or Coulomb interaction is excluded. Among the multiterminal structures, the simplest is a three-terminal T junction (T-J). The sudden opening of transmission into a side terminal attached to a QW may influence the current flow that one wants to measure in the QW in a marked way.^{7,8} In this case, as we show here, the back action of an extra conducting terminal is a single-particle effect and does not require any exotic feature, such as an assistant quasi-bound state in the close vicinity of the T-J.^{9,10} Singularities in the scattering cross section when an extra reaction channel opens have been well studied in the past in the context of nuclear physics and nicknamed Wigner cusp after Wigner.¹¹ The Wigner cusp is extensively described in Refs. 12 and 13 (see also Ref. 14) and is recognized also in nanostructures when coherent charge transport occurs.^{8,15,16} Baranger⁸ studied theoretically conductance in a multiterminal system of crossed quantum wires. Analyzing contributions of separate channels to the conductance, he found a pronounced Wigner cusp when a bend channel was opened by increasing the

Fermi energy. If other channels contribute to the individual transmission with a dip in the conductance, the cusp can be compensated in the total transmission. There is no need of resorting to a specific model for the conductance, as the origin of the singularity at the opening of a channel in a nearby side terminal is simply the interplay between the overall constrain of flux conservation in the scattering across the device and the interference between incoming and reflected wave amplitudes at the junction.

Schult *et al.*¹⁵ set up a self-consistent method to solve the Schrödinger equation and the Poisson equation simultaneously to simulate gate polarization in more complex extended devices. The phenomena we want to address here only appear when lateral quantization occurs, generating subbands in the single-particle spectrum and discrete conduction channels which have a nonlocal quantum influence on the conductance when they are close to threshold.

In this paper we address the simplest tight-binding approach to the threshold problem in a T-J. We show that, when the gate on the side terminal is swept across the pinch-off voltage, an enhancement of the conductance in the measured QW or QPC can occur, which can be turned into a dip, or into other characteristic shapes, by tuning the parameters of the structure. At zero temperature, the singularity appearing in the measured conductance can be a cusp or an inverted cusp, or a saddle point, depending on the relative weight of the tunneling matrix elements which connect the T-J island to the bulk of the quantum wires.

In Sec. II we discuss coherent quantum transport in the simplest T-J between QWs and present the conditions under which the back action of the side terminal can induce a peak or a dip in the source-drain (SD) conductance. In Sec. III we extend our picture to the case of a T-J controlled by gate voltages, which implies that the T-J is effectively turned into an island confined by QPCs. The island is assumed to be large enough, so that charging effects can be ignored but not the quantization of the conductance in the QPCs. In Sec. IV we shortly review the recent experiments on similar devices and we propose to interpret those results at the light of our findings, which do not consider possible many-body correla-

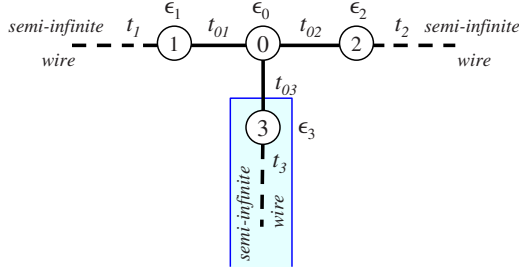


FIG. 1. (Color online) Three-terminal system of one-dimensional semi-infinite atomic chains. The parameters of the tight-binding model are site energies ϵ_i and hopping integrals between neighbor atoms t_{ij} .

tions in action, showing up dramatically at the pinch-off energy of the side terminal.

II. T JUNCTION OF QUANTUM WIRES

To make our argument crystal clear, we first consider a three-terminal system of one-dimensional quantum wires connected at the reference zero site. The formalism we use is straightforward and well established.¹⁷ We assume that source-drain potentials V_1 and V_2 are applied to the electrodes 1 and 2, while the third electrode is gated with gate voltage V_{G3} . The latter is swept across the pinch-off point.

The current flowing from the i th electrode is given, within linear response, by¹⁷

$$I_i = \frac{2e^2}{h} \sum_{j=1}^3 \mathcal{T}_{ij}(V_i - V_j), \quad (1)$$

where

$$\mathcal{T}_{ij} = \int \left(-\frac{\partial f}{\partial E} \right) T_{ij}(E) dE. \quad (2)$$

$T_{ij}(E)$ is the transmission coefficient from the i th to j th electrode for electrons with an incoming energy E and f is the Fermi distribution function. The conductance measured between the electrodes 1 (source) and 2 (drain), in the presence of the electrode 3 left unbiased, is

$$\mathcal{G}_{12,3} = \frac{2e^2}{h} \left(\mathcal{T}_{12} + \frac{\mathcal{T}_{13}\mathcal{T}_{23}}{\mathcal{T}_{13} + \mathcal{T}_{23}} \right) \quad (3)$$

(indices can be interchanged). The second term in Eq. (3) is a contribution from indirect transmission of electrons through the third wire.

As the simplest model, let us assume tight-binding coupling with hopping integrals t_i (taken as real) between neighboring atoms in the i th wire and site energies ϵ_i (see Fig. 1). All calculations are performed exactly within the tight-binding approach.¹⁸ The Green's function g_i in the i th semi-infinite wire is

$$g_i(E) = \begin{cases} \frac{2}{E_i - \sqrt{E_i^2 - 4t_i^2}} & \text{for } E_i < -2|t_i|, \\ \frac{2}{E_i + i\sqrt{4t_i^2 - E_i^2}} & \text{for } |E_i| < 2|t_i|, \\ \frac{2}{E_i + \sqrt{E_i^2 - 4t_i^2}} & \text{for } E_i > 2|t_i| \end{cases} \quad (4)$$

($E_i = E - \epsilon_i$). Hoppings to and from the central zero site at the T-J are denoted by t_{0i} ($i=1,2,3$) and the Green's function of the central site is

$$G_{00} = \frac{1}{E - \epsilon_0 - t_{01}^2 g_1 - t_{02}^2 g_2 - t_{03}^2 g_3}. \quad (5)$$

The Green's functions G_{ij} connecting the electrodes i and j are expressed as

$$G_{ij} = g_i t_{0i} G_{00} t_{0j} g_j. \quad (6)$$

They allow us to calculate the transmission coefficients T_{ij} appearing in Eq. (1) according to¹⁹

$$T_{ij}(E) = v_i v_j |G_{ij}(E)|^2. \quad (7)$$

Here $v_i = \sqrt{4t_i^2 - E_i^2}$ when the relative electron energy in the i th wire E_i enters the wire energy band ($|E_i| \leq 2|t_i|$) and vanishes otherwise. A gate voltage V_{Gi} applied to electrode i shifts its site energies uniformly: $\epsilon_i \rightarrow \epsilon_i - eV_{Gi}$. The pinch-off voltage V_{Gi}^0 makes the Fermi velocity $v_i(E=E_F)$ vanish by moving E_F beyond the bottom of the conduction subband.

To match with some experiments,⁵ as discussed in Sec. IV, we calculate the detector conductance $\mathcal{G}_{12,3}$ (when the source-drain voltage is applied to QW 1 and 2, whereas QW 3 is left unbiased) as well as the conductance $\mathcal{G}_{23,1}$ (when QW 2 and 3 are the current source and drain, respectively, and QW 1 is left unbiased). Conduction in the third wire will start at the pinch-off voltage, for $V_{G3} \geq V_{G3}^0$ with a square-root singularity. The detector conductance $\mathcal{G}_{12,3}$, which, according to Eq. (3), is, at zero temperature,

$$\mathcal{G}_{12,3}^0 = \frac{2e^2}{h} v_1 v_2 t_{01}^2 t_{02}^2 |G_{00}(E_F)|^2 \left[1 + \frac{v_3 t_{03}^2}{v_1 t_{01}^2 + v_2 t_{02}^2} \right] \quad (8)$$

will suffer a back action at the threshold. An appropriate choice of the parameters gives the result of Fig. 2 when the gate voltage is swept across the threshold V_{G3}^0 . The conductance between source and drain, $\mathcal{G}_{12,3}^0$, shows a cusp at the opening of the conduction channel which is rounded off by temperature. The plots show that the width of the Wigner cusp depends on the curvature of the conductance step in $\mathcal{G}_{23,1}$.

In Sec. II B we will show that besides cusps, also dips and saddle points can appear in the source-drain conductance, depending on the actual structure of the T-J which is changed in our model by changing the parameters ϵ_i and t_{0i} .

A. Dependence of the back action on the T-J structure

Let us change the structure of the T-J area by changing the parameters of the model. Here we show that the feature in

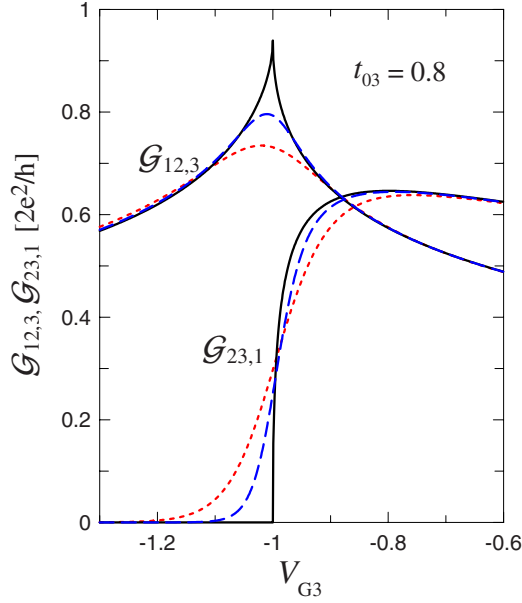


FIG. 2. (Color online) Conductance $\mathcal{G}_{12,3}$ and $\mathcal{G}_{23,1}$ as a function of the swept potential V_{G3} applied to electrode 3. All three wires are assumed to be similar, i.e., $t_i=t=1$ (taken as the energy scale) and $\epsilon_1=\epsilon_2=0$ and $\epsilon_3=-eV_{G3}$. The wires are coupled to each other by the zeroth site (with $\epsilon_0=0$) and the couplings are $t_{01}=t_{02}=0.5$ and $t_{03}=0.8$. The Fermi energy is taken as $E_F=-1$, so that the pinch-off voltage is at $V_{G3}^0=-1$. The plots are for various temperatures: $T=0$ (black solid curve), $T=0.02$ (blue dashed curve), and $T=0.04$ (red dashed curve).

the source-drain conductance $\mathcal{G}_{12,3}$ marking the opening of the conduction channel in the third electrode can take various shapes, specific of the quantum interference occurring in the T-J. To reduce the number of parameters, we will fix the site energies all equal in the rest, $\epsilon_i=0$, and move the Fermi level E_F with respect to these. As before, ϵ_3 will be shifted by sweeping V_{G3} . Let us first assume zero temperature. It is easy to analyze the logarithmic derivatives of $\mathcal{G}_{12,3}^0$ at both sides of the threshold $V_{G3}-V_{G3}^0=0^\mp$. Just below and above the subband threshold $\nu_3=\sqrt{E_{F3}^2-4t_3^2}$ and $\nu_3=\sqrt{4t_3^2-E_{F3}^2}$ vanish, respectively ($E_{F3}=E_F+eV_{G3}$). Correspondingly, from Eqs. (4), (5), and (8), one can get the derivatives in the two limits as follows:

$$\left. \frac{\partial \mathcal{G}_{12,3}^0 / \partial V_{G3}}{\mathcal{G}_{12,3}^0} \right|_{0^-} = t_{03}^2 \operatorname{Re}(G_{00}) \times \frac{E_{F3}}{\nu_3} \text{ for } \nu_3 \rightarrow 0^+,$$

$$\left. \frac{\partial \mathcal{G}_{12,3}^0 / \partial V_{G3}}{\mathcal{G}_{12,3}^0} \right|_{0^+} = t_{03}^2 \left[\operatorname{Im}(G_{00}) + \frac{1}{v_1 t_{01}^2 + v_2 t_{02}^2} \right] \times \frac{E_{F3}}{\nu_3}$$

for $\nu_3 \rightarrow 0^+$. (9)

The derivatives have an explicit singular dependence $1/\nu_3$ or $1/v_3$. The same threshold singularity occurs in the differential cross section for inelastic processes.¹¹⁻¹³ In our situation the scattering problem has also a multichannel structure, and Eq. (9) expresses the change in the interference conditions as well as in the density of available states contributing to the

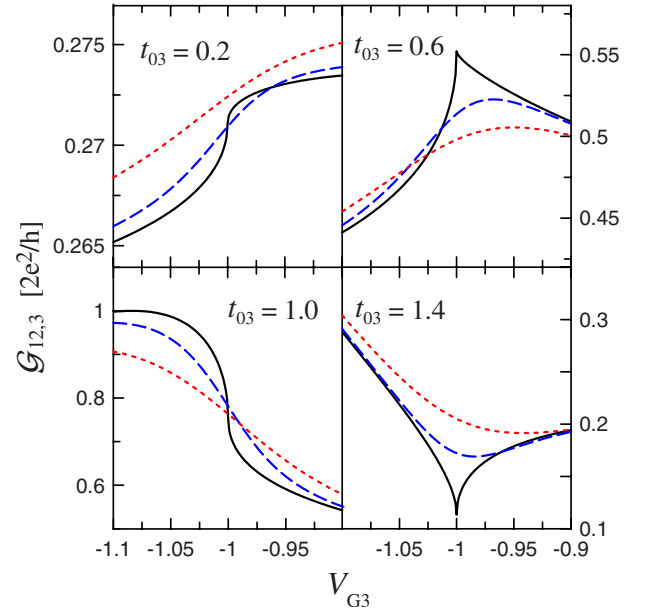


FIG. 3. (Color online) Conductance $\mathcal{G}_{12,3}$ calculated as a function of V_{G3} . The plots are for $t_{03}=0.2$, $t_{03}=0.6$, $t_{03}=1.0$, $t_{03}=1.4$, $\gamma=(t_{01}^2+t_{02}^2)/2=0.25$, and various temperatures: $T=0$ (black solid curves), $T=0.02$ (blue dashed curves), and $T=0.04$ (red dotted curves). The other parameters are taken as in Fig. 2.

linear conductance at the Fermi energy when the gate voltage V_{G3} just opens the new channel in the side terminal 3 to conduction.

Since, above the threshold, $\operatorname{Im}(G_{00})<0$, the derivative $\partial T_{12}/\partial V_{G3}|_{0^+}$ is always negative. However, the derivative $\partial \mathcal{G}_{12,3}^0/\partial V_{G3}|_{0^+}$ can be negative or positive due to the presence of the back reflection from the third wire [the second term appearing in Eq. (3)]. In particular, if the transmissions T_{13} and T_{23} of Eq. (7) have opposite slopes at the threshold, a peak develops. Figure 3 shows different shapes for the singularity in $\mathcal{G}_{12,3}^0$ close to the threshold voltage. To simplify our approach even further, we assume that the wires are equal, i.e., they have equal hopping integrals $t_1=t_2=t_3=t$ and define $E_0^r=E_F-\epsilon_0+t_{03}^2/|t|$, the renormalized energy of an electron at the zeroth site, and $\gamma=(t_{01}^2+t_{02}^2)/2t^2$. The shape of the singularity in Fig. 3 depends on the relative couplings t_{0i} . In particular we choose the symmetric case ($t_{01}=t_{02}$), so that the dependence is on t_{03} and $\gamma=(t_{01}^2+t_{02}^2)/2$ only. Together with upward and downward cusps, saddle-point singularities can appear. Equation (9) implies that $\partial \mathcal{G}_{12,3}^0/\partial V_{G3}>0$ when

$$E_0^r < \gamma E_F \text{ for } V_{G3} - V_{G3}^0 \rightarrow 0^-,$$

$$E_0^{r2} - 2\gamma E_0^r E_F + 2\gamma^2 E_1^2 < 4t^2 \gamma^2 \text{ for } V_{G3} - V_{G3}^0 \rightarrow 0^+.$$

(10)

Figure 4 represents the boundaries for these various possibilities in the space of the parameters E_F and E_0^r when $\gamma=0.25$. The left-hand side of the diagram corresponds to an n -doped semiconducting structure, while the right-hand side corresponds to the p -doped case. This means that the Wigner cusp should be easier detected in an electron system (when

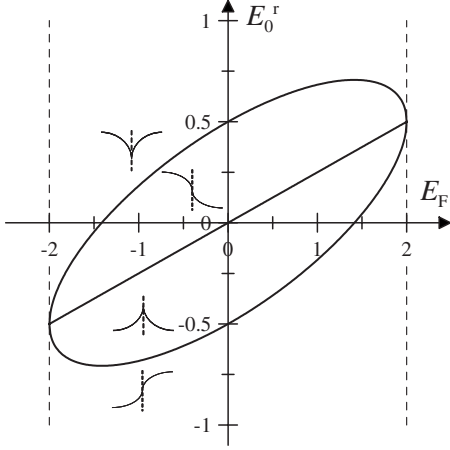


FIG. 4. Diagram showing regions with different singularities of the zero-temperature conductance $\mathcal{G}_{12,3}^0$. The derivative $\partial\mathcal{G}_{12,3}^0/\partial V_{G3}|_{0^+}$ (that one above the threshold voltage V_{G3}) is negative inside the ellipse $E_0^r{}^2 - 2\gamma E_0^r E_F + 2\gamma^2 E_F^2 = 4t^2\gamma^2$, whereas outside the ellipse its value is positive. The line $E_0^r = \gamma E_F$ separates regions with different signs of the derivative of the conductance in the subthreshold regime. $\partial\mathcal{G}_{12,3}^0/\partial V_{G3}|_{0^-} < 0$ above the line, whereas it is positive below this line. In the model $-2 \leq E_F \leq 2$ (E_F is between the dashed lines). The plot is done for $\gamma = 0.25$.

E_0^r is negative), whereas the dip should be more common in a hole system.

We now shortly discuss the possibility that a bound state splits off the subband threshold of wire 3 in our tight-binding model and the consequences on $\mathcal{G}_{12,3}^0$. The term $-t_{03}^2 g_3$, appearing in the denominator of the central-site Green's function G_{00} of Eq. (5), shifts the energy of the central site ϵ_0 . This term is due to back reflection from wire 3 and, being positive for $E_{F3} < -2|t_3|$ (as $g_3 < 0$ below the band edge), it shifts the zero-site energy downward. When ϵ_0 is moved below the band edge, G_{00} acquires a pole on the real energy axis, which signals the presence of a bound state localized at the center of the structure. However, we find that G_{00} has no poles for any value of $E_{F3} < -2|t_3|$ and t_{03} in our model. This means that no applied gate potential V_{G3} can give a bound state in the subthreshold region. However, if $|E_{F3}| < 2|t_3|$, one could find such a pole in G_{00} when

$$V_{G3} = -[E_F(1 - \gamma) - \epsilon_0] \frac{2t_3^2}{t_{03}^2} \quad (11)$$

provided $|E_F(1 - \gamma) - \epsilon_0| < t_{03}^2/|t_3|$. In addition, less stringent conditions for the occurrence of a subthreshold bound state could be realized by adding side gates in the model, which have the role of sharpening the electron confinement close to the central island (see Sec. III). Nevertheless, analyzing many plots of $\mathcal{G}_{12,3}$ for various sets of parameters, we did not find any peculiar feature induced by the pole. Had we allowed for the center of the bands of electrodes 1 and 2 to be shifted, we could have found a localized zero-site state embedded with the continuum of propagating states from source to drain. This could produce the characteristic Fano-type resonant peak in the source-drain conductance, which could

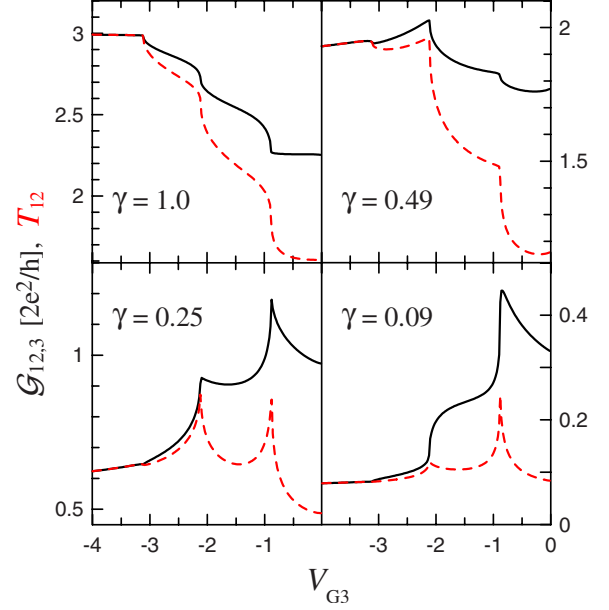


FIG. 5. (Color online) Zero-temperature conductance $\mathcal{G}_{12,3}^0$ (black solid curve) and transmission T_{12} (red dashed curve) vs the gate potential V_{G3} for the quantum wires of the width $M_1 = M_2 = M_3 = 4$. The plots are for various symmetric couplings: $\gamma = (t_{01}^2 + t_{02}^2)/2 = 1$, $\gamma = 0.49$, $\gamma = 0.25$, and $\gamma = 0.09$, while $t_{03} = 1$ in all cases. Other hopping integrals are taken as $t = 1$, the site energies as $\epsilon_i = 0$, $E_F = -0.5$, and $T = 0.5$.

even overlap with the threshold effect considered in this work.

B. Multichannel conductance

Up to now the conductance due to a single channel was considered. In the multichannel case, one can expect that opening successive channels adds further quantum interference in the back reflection at the T-J. The transmission coefficients are expressed by

$$T_{ij} = \sum_{k_i, k_j} T_{k_i, k_j}, \quad (12)$$

where the summation runs over all incoming and outgoing channels in the wires i and j (with wave vectors k_i and k_j , respectively). They have been calculated along the lines described in the Appendix. Figure 5 shows plots of $\mathcal{G}_{12,3}^0$ vs the sweeping gate voltage V_{G3} for a number of channels $M_i \leq 3$. They are fully open from source to drain while V_{G3} controls the successive openings in wire 3. In the subthreshold region, the case for $\gamma = 1$ corresponds to an ideal SD wire and the conductance at the plateaux reaches $3 \times 2e^2/h$. The dashed curve refers to the direct SD transmission T_{12} which is controlled by γ , while the full curve refers to $\mathcal{G}_{12,3}^0$ and includes also the indirect contributions when current flows also in wire 3, according to Eq. (3). As expected, $\mathcal{G}_{12,3}^0$ is reduced in the top plots, for high γ , when successive channels are opened in the third wire. As in the one-channel case, the Wigner cusp occurs for $\gamma \ll t_{03}$. The threshold singularities are more pronounced at successive openings, where the interference effect builds up more strongly.

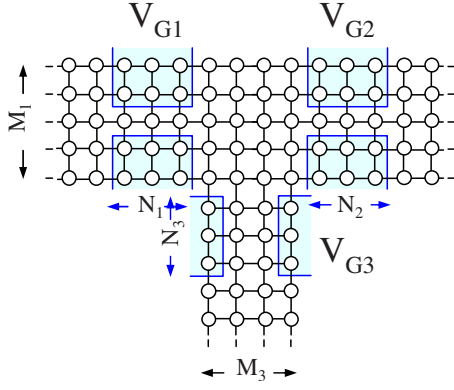


FIG. 6. (Color online) Modeling of the three-terminal system with QPCs with M_i channels. The shaded area shows the region, including N_i sites, where the gate potential V_{G_i} squeezes the constriction by moving the site energies ϵ_i above the conduction band (see the inset in Fig. 7).

III. T JUNCTION OF QPCs CONTROLLED BY GATE VOLTAGES

Voltage gates V_{G_i} can tune the T junction ($i=1,2,3$ labels the terminal as previously) and control the QPCs confining a central island at the crossing, as sketched in Fig. 6. The area is large enough, so that no charging effect is expected within the island. We model this case by extending our tight-binding approach for M_i -channel wires. The gate voltages shift N_i -site energies close to the T crossing, as explained in the Appendix. If we pinch off the side terminal by choosing $V_{G_3}=-1.2$ and we switch off the second gate by putting $V_{G_2}=0$, just one QPC, along the SD path, is left. Figure 7 shows the quantization of the QPC conductance \mathcal{G}_{12}^0 vs the gate voltage V_{G_1} . The inset shows how the lateral confine-

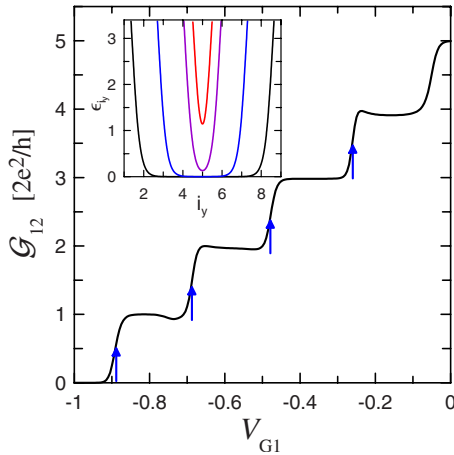


FIG. 7. (Color online) Conductance \mathcal{G}_{12}^0 through a single QPC in a quantum wire as a function of the gate potential V_{G_1} . The arrows show the voltages $V_{G_1}=-0.89, -0.69, -0.48,$ and -0.26 at which we perform further conductance studies when channels from the side terminal are open (the results are presented in Figs. 8 and 9). The inset shows the site energies ϵ_{i_y} along the cross section of the QPC for $V_{G_1}=-0.2, -0.5, -0.8,$ and -0.9 (from edge to center: black, blue, purple, and red curves). The size of the wires is $M_1=M_2=9$ and the length of the constriction is $N_1=3$. $E_F=-1.5$ and $T=0$.

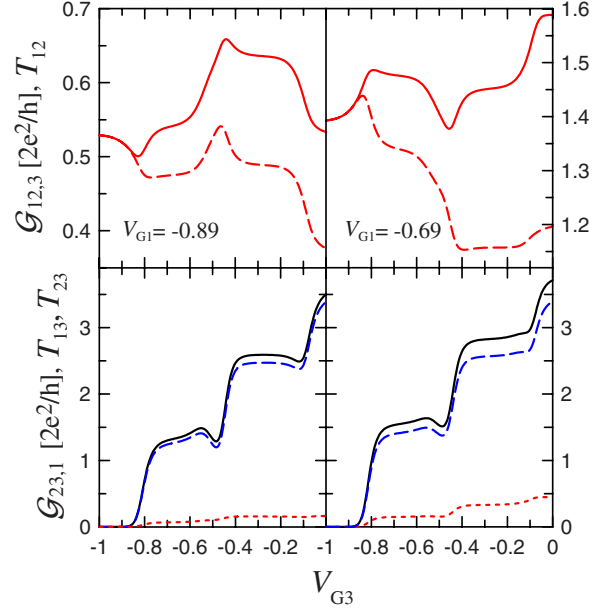


FIG. 8. (Color online) Top panels: $\mathcal{G}_{12,3}^0$ (red full line) and T_{12} (red dashed lines). Bottom panels: $\mathcal{G}_{23,1}^0$ (black full line), T_{13} (blue dashed line), and T_{23} (red broken line) vs V_{G_3} for $V_{G_1}=-0.89$ (right), -0.69 (left), and $V_{G_2}=0$. The length of QPCs are $N_1=N_2=N_3=3$, the width of the wires are $M_1=M_2=9$, and $M_3=5$. (Other parameters are $t_i=t_{01}=t_{02}=t_{03}=1$, $E_F=-1.5$, and $T=0$).

ment increases in our model (see the Appendix) by cranking V_{G_1} . The site energies ϵ_{i_y} on the lateral sites i_y are moved increasingly upward away from the center of the QW.

By changing V_{G_3} , we consecutively open the channels in the side terminal 3. If we take the source QPC as opened, with the conductance at one of the plateaus of Fig. 7 by opening the side terminal with V_{G_3} , the conductance $\mathcal{G}_{12,3}^0$ can develop a saddle-point singularity at the threshold. More interesting is the situation when the source QPC is polarized such that the initial SD conductance is between successive plateaux (see arrows in Fig. 7). Then one can expect different threshold features (with cusps and dips) in the SD conductance when the channels in the side terminal 3 are opened to conduction. Figures 8 and 9 present the results at these values: $V_{G_1}=-0.89, -0.69$ and $V_{G_1}=-0.48, -0.26$, respectively. The transmission coefficient T_{12} is plotted together with $\mathcal{G}_{12,3}^0$ in the top panels (dashed line) and T_{13} and T_{23} appear in the bottom panels together with $\mathcal{G}_{23,1}^0$ (broken lines) to show the various contributions of direct and indirect transmissions. The closer the source QPC is, the smaller becomes the contribution to $\mathcal{G}_{23,1}^0$ coming from T_{23} . It is interesting that T_{12} shows an alternating behavior at the lower openings which is reflected in the SD conductance. At $V_{G_1}=-0.89$ the pattern is dip-peak-dip, while at $V_{G_1}=-0.69$ the pattern is peak-dip-peak. In decreasing V_{G_1} further, the pattern is less clear, but alternation can still be seen in the SD conductance. Of course, when the source QPC becomes more and more transparent (Fig. 9), the back action due to the sweeping of V_{G_3} is weaker. When this happens, the peaks tend to fade away and the dips prevail.

Finally, we concentrate on the first threshold for the conductance in the third QPC, $\mathcal{G}_{23,1}^0$, assuming that just one

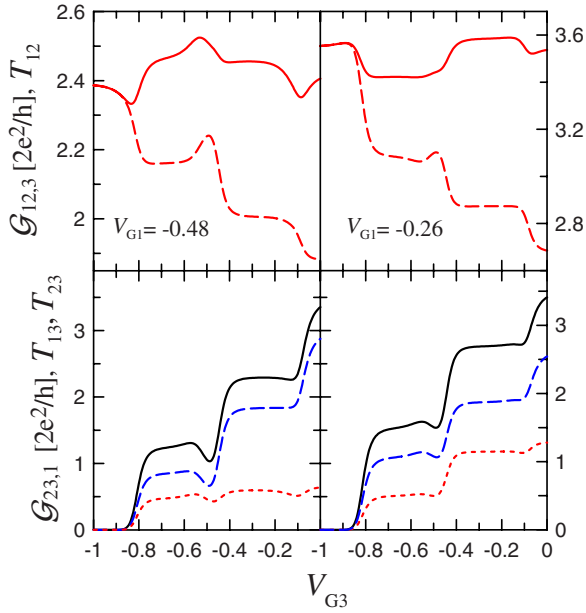


FIG. 9. (Color online) Same as Fig. 8 for $V_{G1} = -0.48$ (left) and -0.26 (right). Other parameters are as in Fig. 8.

channel can be only activated ($M_i = 1, i = 1, 2, 3$) and test the conductances with strong asymmetric polarization of the source and drain QPCs (see Fig. 10). We keep the gate voltage of the drain fixed at $V_{G2} = -1.5$ and compare the case when the source QPC is polarized at $V_{G1} = -5.0$ (top panels) with the case of $V_{G1} = -0.2$ (bottom panels) ($N_1 = N_2 = 1$). In sweeping across the conductance threshold the gate voltage

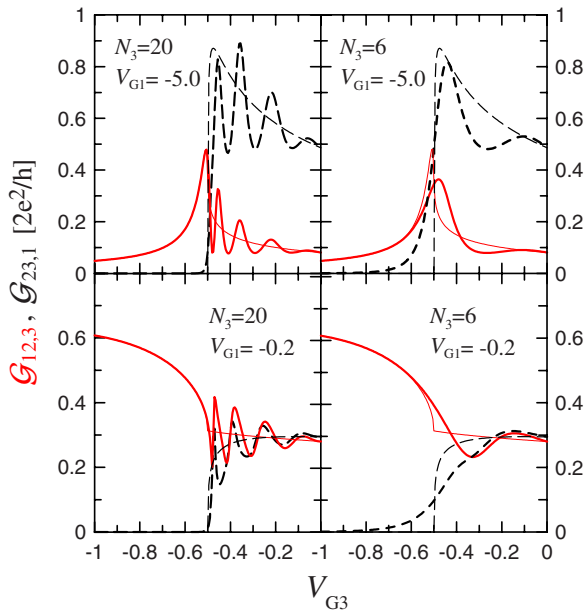


FIG. 10. (Color online) Conductances $G_{12,3}^0$ (red solid curve) and $G_{23,1}^0$ (black dashed curve) vs V_{G3} for a one-dimensional system with QPCs. The gate voltages are $V_{G2} = -1.5$ and $V_{G1} = -5$ (top) and -0.2 (bottom). The length of QPCs are $N_1 = N_2 = 1$ and $N_3 = 20$ (left panels) and 6 (right panels). The thin curves show the results for $N_3 = \infty$. The other parameters are $t_{01} = t_{02} = t_{03} = 1$, $E_F = -1.5$, and $T = 0$.

on the side terminal V_{G3} , we compare various spatial extensions of the third gate ($N_3 = \infty, 20, 6$). The SD conductance $G_{12,3}^0$ (red online) is quite small when the source QPC is close to the pinchoff ($V_{G1} = -5.0 < V_{G2}$), except in the neighborhood of the threshold for $G_{23,1}^0$ (black online), where it has a peak (top panels). In the opposite case ($V_{G1} = -0.2 > V_{G2}$), the SD conductance $G_{12,3}^0$ has a dip at the threshold and stabilizes at a lower value (bottom panels). With the polarizations chosen, the T terminal becomes a fork and the current incoming from the source QPC is divided between terminals 2 and 3 almost equally.

As the system is effectively one dimensional ($M_i = 1$), resonance oscillations appear in the conductance $G_{23,1}^0$ at the opening of the channel in terminal 3, as can be expected from textbook exercises when the transmission is calculated with an incoming energy just above the top of a barrier. The oscillations squeeze close to threshold with increasing of the barrier extension (i.e., increasing N_3), until they merge together for $N_3 = \infty$ (thin black line) when V_{G3} is applied to the whole wire 3. These oscillations produce a back action on the SD conductance $G_{12,3}^0$ which oscillates as well, with a phase delay.

IV. CONCLUDING REMARKS

Multiterminal nanostructures involving QPC are playing an increasing role in the fabrication of quantum coherent devices to be used in building qubits for quantum computation. Also, spintronics requires spin filters which could be controlled by magnetic fields or by gate voltages provided the charge current is carefully tuned and intrinsic (e.g., Dresselhaus) and extrinsic (impurity driven or Rashba) spin-orbit couplings can be exploited. On the other hand, nanoconstrictions offer a privileged ground for the action of electron-electron correlations and it is often difficult to separate their effects from those of single-particle quantum interference in coherent transport. As QPC can be used as detectors, a reliable interpretation of the results requires that the two classes of phenomena are satisfactorily sorted out.

We have reconsidered the quantum conductance in a T-junction structure within a single-particle linear-response scattering approach. We have used the simplest tight-binding model to provide a complete picture of how the conductance can be changed at the threshold of side terminals by tuning the gate voltages which confine the ballistic transport of the electrons. Our emphasis has been on the effects that could be measured on the main source-drain conductance or on the conduction in the side terminal channel that is opened.

Our model reproduces the measuring setup of some recent experiments.^{5,6} Two separate types of conductance measurements were reported. In the first one, the conductance $G_{23,1}$ of a QPC (from terminal 2 to terminal 3, nicknamed “swept” QPC) was measured, while sweeping the gate voltage V_{G3} . Voltages applied to other QPCs were held fixed, including those controlling the conductance from terminal 1 to terminal 2 (nicknamed “detector” channel). In the second measurement, the voltage applied to the gate V_{G3} of the swept QPC was again varied over the same range. However, its Ohmic contacts were left unbiased, while a SD current was

driven through the detector channel and the conductance $\mathcal{G}_{12,3}$ was measured. From these two separate measurements, the variation of the detector conductance $\mathcal{G}_{12,3}$ could be correlated with that of the swept wire $\mathcal{G}_{23,1}$ as a function of V_{G3} . The experiments showed an asymmetrical peak in the detector conductance $\mathcal{G}_{12,3}$, just after the pinch-off gate voltage⁵ or before this point.⁶ On the basis of our results, we can interpret these experimental features as due to the threshold effect in single-particle quantum interference. This can be expected at each opening of the channel. We have showed that the cusp in the conductance could be replaced by a dip, or a saddle point, depending on the polarization of the voltage gates. If the detector QPC is kept rather open, with the conductance close to the quantum conductance $2e^2/h$ (or its multiple), then the conductance is reduced at the pinch-off voltage and displays a saddle-point singularity. We suggest controlling the shape of the conductance singularity occurring in the detector QPC conductance at the sweeping of the swept channel by changing its gate voltages. When the conductance of the swept channel moves across the successive conductance plateaux, the threshold conductance peak in the detector channel may change from cusp to dip, with small changes in the polarization of its gates.

Our model is for free electrons and it does not include, nor require, any kind of charging of the central area. Of course, we cannot exclude that a small size area for strongly confined electrons is formed in correspondence with the pinch-off gate of the swept QW. In this case a proper lateral quantum dot would form and Coulomb blockade would dictate its occupancy. The detector wire could detect the extra charge or even undergo resonant tunneling of Fano type. The reported shift⁶ with increasing in-plane magnetic field could be due to the first two addition energies in the quantum dot and support the charging interpretation. However, we are more in favor of the threshold effect explanation. Often the peak was measured at temperature $T \gtrsim 1.8$ K when the size of the wires used in the experiment should not lead to dramatic Coulomb effects. On the other hand it is rather hard to recognize a Zeeman splitting of the peak from the data, especially at low magnetic field, while, when the magnetic field increases considerably, one cannot exclude little uncontrolled orbital effects. In any case, we believe that the experimentally observed phenomenon should first be confronted with our interpretation before more exotic arguments implying electron-electron correlations at the QPC constriction are invoked.

ACKNOWLEDGMENTS

We would like to acknowledge fruitful discussions with Jonathan Bird on his experiments and with Benoit Jouault, as well as technical assistance in calculations by Jakub Łuczak. This work was supported as a part of the European Science Foundation EUROCORES Programme FoNE by funds from the Ministry of Science and Higher Education and EC 6FP (Contract No. ERAS-CT-2003-980409).

APPENDIX: MULTICHANNEL QW AND QPC

In Sec. II we considered a three-terminal (T-shape) system of one-dimensional semi-infinite atomic chains (as depicted

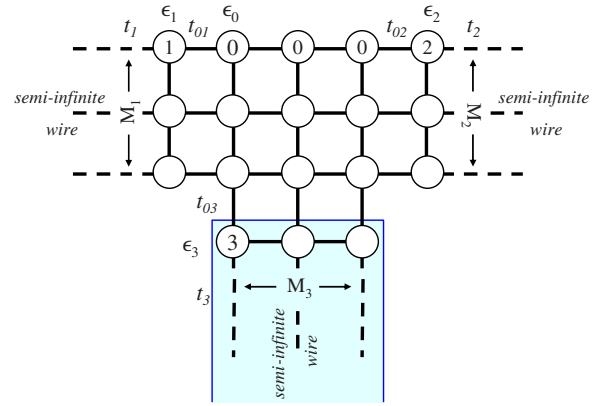


FIG. 11. (Color online) The tight-binding model of three coupled quantum wires used for transport studies of the threshold effect in the multichannel case.

in Fig. 1) and its extension to the multichannel case. In Sec. III gates were added onto the wires to tune conductance as in QPCs.

To extend the tight-binding model to a multichannel device, we have used a method proposed by Ando,²⁰ which was extensively applied in theoretical studies of electronic transport in nanostructures. Our three terminal system is modeled as three semi-infinite stripes of atoms of width $M_i a$ ($i=1, 2$, and 3 for the three QWs) (see Fig. 11) (a is the lattice constant taken as unity in the calculations). Here $m_i=1, \dots, M_i$ labels the discrete lattice sites in the transverse y direction with respect to the current flow and the modes confined in the transverse direction are labeled by the wave vectors $k_i = \pi n_i / (M_i + 1)a$ with $n_i=1, \dots, M_i$. Wave functions for the lateral confinement are $X_{k_i}(m_i) = \sqrt{2/(M_i + 1)} \sin(k_i m_i a)$. They correspond to the energy dispersion $\epsilon_i + 2t_i \cos k_i a$. The transmission coefficients $T_{k_i k_j}$, from the k_j to the k_i channel, are as follows:

$$T_{k_i k_j} = v_{k_i} v_{k_j} \left| \sum_{m_i=1}^{M_i} \sum_{m_j=1}^{M_j} X_{k_i}(m_i) G_{ij}(m_i, m_j) X_{k_j}(m_j) \right|^2 \quad (\text{A1})$$

with $v_{k_i} = \sqrt{4t_i^2 - (E_i - 2t_i \cos k_i a)^2}$ for $|E_i - 2t_i \cos k_i a| \leq 2|t_i|$ and zero otherwise. $G_{ij}(m_i, m_j)$ denote matrix elements of the Green's function in the site representation, connecting atoms in the first row of the i and j wires, respectively. In the semi-infinite ideal wire i , the Green's function is expressed as

$$G_{ii}(m_i, m'_i) = \frac{2}{M_i + 1} \sum_{k_i} \sin(k_i m_i a) \sin(k_i m'_i a) \times g_i(E_i - 2t_i \cos k_i a), \quad (\text{A2})$$

where g_i is given by Eq. (4). The matrix elements G_{ij} are calculated by a direct matrix inversion.

Now we want to apply voltage gates at limited portions of the wires close to the T-J to model QPCs. This model is closer to the experiments, in which electronic transport was controlled by a system of several gate electrodes forming QPCs that confine a central island. Applying a negative gate potential V_{Gi} , one can control the size of the QPC and reduce the number of transverse modes participating in the transmission. The gate potential forms a potential barrier in the constriction, which depends on the transverse coordinate. Models of semiconducting nanostructures and studies of the current flow inside them are well developed (see, for example, Refs. 17 and 21). For our purpose, we assume the potential barrier inside the QPC to be uniform and constant along the constriction, with a simple transverse shape.²² The site energies at sites i_y , in the region covered by the gate, are

$$\epsilon_{i_y} = U_0 \left\{ \frac{1}{e^{(i_y a + w_i) \alpha} + 1} + \frac{1}{e^{-[i_y a - (M_i + 1)a - w_i] \alpha} + 1} \right\}, \quad (\text{A3})$$

where $w_i = -eV_{Gi}M_i a / 2t + a/2$ and α describes the slope of the potential. We take $U_0 \gg |t|$ in order to shift ϵ_i above the conduction band. The potential V_{Gi} is normalized in such a way that the QPC is closed at $V_{Gi} = -1$, whereas a perfect transmission occurs for $V_{Gi} = 0$. We have checked that the results do not depend significantly on the potential shape. If the potential drop is sharp and all the site energies are equal inside the QPC, $\epsilon_{i_y} \approx 0$, then the conductance plateaux become flat and uniform, as expected for quantization at low temperatures.

-
- ¹M. Field, C. G. Smith, M. Pepper, D. A. Ritchie, J. E. F. Frost, G. A. C. Jones, and D. G. Hasko, *Phys. Rev. Lett.* **70**, 1311 (1993); E. Buks, R. Schuster, M. Heiblum, D. Mahalu, and V. Umansky, *Nature (London)* **391**, 871 (1998); L. P. Kouwenhoven, D. G. Austing, and S. Tarucha, *Rep. Prog. Phys.* **64**, 701 (2001); J. R. Petta, A. C. Johnson, C. M. Marcus, M. P. Hanson, and A. C. Gossard, *Phys. Rev. Lett.* **93**, 186802 (2004); L. DiCarlo, H. J. Lynch, A. C. Johnson, L. I. Childress, K. Crockett, C. M. Marcus, M. P. Hanson, and A. C. Gossard, *ibid.* **92**, 226801 (2004); A. C. Johnson, C. M. Marcus, M. P. Hanson, and A. C. Gossard, *ibid.* **93**, 106803 (2004).
- ²P. Debray, V. Zverev, O. Raichev, R. Klesse, P. Vasilopoulos, and R. S. Newrock, *J. Phys. Condens. Matter* **13**, 3389 (2001); M. Yamamoto, M. Stopa, Y. Tokura, Y. Hirayama, and S. Tarucha, *Science* **313**, 204 (2006).
- ³K. Hitachi, M. Yamamoto, and S. Tarucha, *Phys. Rev. B* **74**, 161301(R) (2006).
- ⁴V. S. Khrapai, S. Ludwig, J. P. Kotthaus, H. P. Tranitz, and W. Wegscheider, *Phys. Rev. Lett.* **97**, 176803 (2006).
- ⁵T. Morimoto, Y. Iwase, N. Aoki, T. Sasaki, Y. Ochiai, A. Shailos, J. P. Bird, M. P. Lilly, J. L. Reno, and J. A. Simmons, *Appl. Phys. Lett.* **82**, 3952 (2003); see also J. P. Bird and Y. Ochiai, *Science* **303**, 1621 (2004).
- ⁶Y. Yoon, L. Mourokh, T. Morimoto, N. Aoki, Y. Ochiai, J. L. Reno, and J. P. Bird, *Phys. Rev. Lett.* **99**, 136805 (2007).
- ⁷L. Worschech, B. Weidner, S. Reitzenstein, and A. Forchel, *Appl. Phys. Lett.* **78**, 3325 (2001).
- ⁸H. U. Baranger, *Phys. Rev. B* **42**, 11479 (1990).
- ⁹B. R. Bułka, M. Tolea, and I. V. Dinu, *Phys. Rev. B* **74**, 205301 (2006).
- ¹⁰V. I. Puller, L. G. Mourokh, A. Shailos, and J. P. Bird, *Phys. Rev. Lett.* **92**, 096802 (2004).
- ¹¹E. P. Wigner, *Phys. Rev.* **73**, 1002 (1948).
- ¹²R. G. Newton, *Scattering Theory of Waves and Particles* (Springer-Verlag, New York, 1982), Chap. 17.2.
- ¹³L. D. Landau and E. M. Lifschitz, *Quantum Mechanics*, 3rd ed. (Pergamon, Oxford, 1977), Chap. 18.
- ¹⁴L. M. Delves, *Nucl. Phys.* **8**, 358 (1958); H. Hotop, M.-W. Ruf, and I. I. Fabrikant, *Phys. Scr.* **110**, 22 (2004); J. Weiner, V. S. Bagnato, S. Zilio, and P. S. Julienne, *Rev. Mod. Phys.* **71**, 1 (1999).
- ¹⁵R. L. Schult, D. G. Ravenhall, and H. W. Wyld, *Phys. Rev. B* **39**, 5476 (1989); D. G. Ravenhall, H. W. Wyld, and R. L. Schult, *Phys. Rev. Lett.* **62**, 1780 (1989).
- ¹⁶M. Büttiker, Y. Imry, R. Landauer, and S. Pinhas, *Phys. Rev. B* **31**, 6207 (1985).
- ¹⁷D. K. Ferry and S. M. Goodnick, *Transport in Nanostructures* (Cambridge University Press, Cambridge, 1997).
- ¹⁸E. N. Economou, *Green's Functions in Quantum Physics*, 3rd ed. (Springer-Verlag, Berlin, 2006).
- ¹⁹D. S. Fisher and P. A. Lee, *Phys. Rev. B* **23**, 6851 (1981).
- ²⁰T. Ando, *Phys. Rev. B* **44**, 8017 (1991).
- ²¹S. E. Laux and F. Stern, *Appl. Phys. Lett.* **49**, 91 (1986); S. E. Laux, A. Kumar, and M. V. Fischetti, *IEEE Trans. Nanotechnol.* **1**, 255 (2002); *J. Appl. Phys.* **95**, 5545 (2004).
- ²²A. Weisshaar, J. Lary, S. M. Goodnick, and V. K. Tripathi, *J. Appl. Phys.* **70**, 355 (1991).